# Secondary structure of muramyl dipeptide glycoside in pristine state and immobilized on nanosilica surface

Liana R. Azizova[†♯*], Tetiana V. Kulik[†], Borys B. Palianytsia[†], German M. Telbiz[‡], Mykola T. Kartel[†]

[†]Chuiko Institute of Surface Chemistry, National Academy of Sciences of Ukraine, 17 Generala Naumov Str., Kyiv 03164, Ukraine. [*]Corresponding author: e-mail address: liana.azizova@yahoo.com
[‡]L. V. Pisarzhevsky Institute of Physical Chemistry National Academy of Sciences of Ukraine, Nauky Av. 31, Kyiv 03039, Ukraine.
[♯]Cardiff University, Heath Park, Cardiff, CF14 4XY

*KEYWORDS. Temperature programmed desorption mass spectrometry (TPD-MS), muramyl dipeptide, fumed silica, β-turn, Fourier transform infrared spectroscopy (FT-IR), pyrolysis, adjuvants, immunostimulatory agents*

**ABSTRACT:** Fourier transform infrared spectroscopy (FT-IR) and temperature programmed desorption mass spectrometry (TPD-MS) data of *O*-glycoside MDP in pristine and immobilized on silica surface states indicate that *O*-glycoside MDP binds to the silica surface by means of carboxylic and NH moieties of isoglutamine. Moreover, pyrolysis of *O*-glycoside MDP on the silica surface proceeds through formation of additional product 3-iminopyridine-2(3H)-one, which identified in mass spectra as molecular ion with *m/z* 108 and its fragment ions with *m/z* 79, 77, 51. FTIR and TPD-MS data confirm existence of a MDP first β-turn on the silica surface resulting from the formation of a hydrogen bond between the NAc carbonyl and the *L*-Ala NH for MDP and its analogs, as reported previously.

## INTRODUCTION

Glycopeptides play an important role in various biological processes such as cellular recognition, immune response, cell growth, cell adhesion and inflammation [1]. Muramyl dipeptide (MDP) is a glycopeptide, the minimal active fragment of peptidoglycan, which possess all its main properties. It is well known that biological and physicochemical functions of glycopeptides require their distinct conformational features. MDP is consists of carbohydrate residue of *N*-acetylmuramic acid and dipeptide *L*-alanyl-*D*-isoglutamine. MDP and its derivatives possess adjuvant, anti-infectious and antitumor activities, activates immunocompetent cells [2, 3] as their specifically recognized by the pathogen recognition receptor molecule NOD2 (nucleotide-binding oligomerization domain-containing protein 2) [4]. NOD2 regulates cytokine, chemokine, and antimicrobial peptide production and therefore involved in both adaptive and innate immune systems. Despite that adjuvants are vital components of certain inactivated vaccines only a few adjuvants licensed for use in human vaccines [5]. Therefore, creation of new and safe adjuvants is important aim in vaccine development as existing adjuvants are poor inducers of Th1-type of cellular immune responses [5]. The Modern Covid-19 pandemic revealed of utmost demand in safe and effective vaccines. However, MDP toxicity hinders its use in vaccines. Efforts of scientists are focused on the synthesis nontoxic, nonpyrogenic derivatives of MDP with desirable properties.

Novel nanotechnology-based vaccine strategies are the promising way for development advanced vaccines with the induction of immune responses against infectious diseases including intranasal drug delivery systems [6-8]. Nanomaterial that used as controllable delivery systems could be organic (biopolymers/polymers, liposomes, micelles, etc.), inorganic (metal oxides, gold nanoparticles, etc.), carbon-based and hybrid organic-inorganic materials [6-8]. Nanomaterials based on silica and alumina have unique acid-base surface properties, a smaller particle size, improved stability, and easily functionalizable structure [9, 10]. Therefore, on their basis, a number of attractive drug/vaccine delivery systems were obtained [11-15].

Silica is attractive adjuvant candidate due to its unique properties such as tunable structural properties, adsorption of specific biomolecules, low cytotoxicity, easy functionalization ability and molecule anchoring, and potential ability to act as delivery vehicles for a variety of immunostimulatory agents [16, 17]. The modification of the fumed silica surface with organic moieties

may result in controlled release and molecular recognition capabilities of fumed silica for drug delivery and biosensing applications, respectively [18-24]. Fumed silica can serve as carrier of medicines, allowing convenient transport of the active component into the body. Earlier, researchers used silica as a platform for delivery glucosaminylmuramyl dipeptide (GMDP) to treat endometriosis [25]. GMDP is a synthetic MDP derivative applied for treatment of secondary immunodeficient disorders [25]. The topical delivery of GMDP immobilized on the (3-Aminopropyl)triethoxysilane (APTES)-modified silica nanoparticles significantly enhances drug effect on the macrophages and its phagocyte activity, whereas the immobilization of GMDP on unmodified silica nanoparticles leads to loss of immunomodulatory effect of GMDP. The authors [25] explain loss of the immunomodulatory effect of GMDP on the silica by inactivating of binding sites of GMDP responsible for its pharmacological activity due to adsorption on the unmodified silica or conformational changes of the drug molecule. In a similar way, interaction of MDP with silica surface and its conformational changes can influence on immunomodulatory effect of MDP.

The $^{13}$C-NMR and $^{1}$H-NMR studies of MDP indicate the possible existence of non-random structures in solution [26-29]. Fermandjian and co-workers [30, 31] proposed that in DMSO solution MDP is consists of two type II adjacent β-turns forming an S-shaped structure. According to them first β-turn is formed by a $C_{10}$ hydrogen bonding between the Ala NH and the acetamido C=O of N-acetylmuramic acid. Existence of second β-turn assumes presence of a free carboxamide group of isoglutamine. The existence of the first β-turn is supported by the nuclear Ovrhauser effect spectroscopy and the H-bond between Ala-NH and the acetamido C=O by the temperature coefficient of the Ala-NH proton chemical shift. The second β-turn was proposed on the ground of $^{1}$H-$^{1}$H coupling constants, while the H-bond between $NH_2$ group of carboxamide moiety of isoglutamine and C=O of lactoyl fragment was not consistent with the temperature-dependence coefficients of the resonances [30, 31]. Molecular dynamic calculations were used to confirm the presence of the first β-turn [32], however it was found that the presence of the second β-turn was less advantageable [33, 34]. There is no clear understanding of the MDP conformational structure.

Nuclear magnetic resonance (NMR) techniques and molecular dynamics are the most common and widely used techniques to study the conformational features of MDP derivatives, immobilization on surfaces also can be studied using temperature-programmed desorption mass spectrometry (TPD-MS) to differentiate processes with various activation parameters [35-37]. Infrared (IR) spectroscopy is an important method for the identification surface groups, determination their structure and nature of appeared bonds. Also, IR spectroscopy is well established experimental technique for the analysis of secondary structure of polypeptides and proteins in solution and in adsorbed state [38, 39]. It was interesting to examine by TPD-MS and IR-spectroscopy if MDP *O*-glycoside would adopt the same bound state in pristine state and adsorbed on silica surface that influence on conformational structure as MDP in DMSO and water. The interaction of MDP *O*-glycoside with silica can influence its bioactivity as spatial organization of biomolecules determine their biological activity. Hence, the presented work reports the results of our investigation on interaction of MDP *O*-glycoside with silica surface for the determination of the binding mechanism and adsorption complexes structure by TPD-MS and IR-spectroscopy. The obtained data and knowledge are important for the understanding binding mechanisms of MDP and its derivatives to the carrier active sites for the design MDP-delivery systems.

*EXPERIMENTAL SECTION*

*Samples.* Silicon dioxide with the specific surface area of 270 $m^2$/g (Kalush, Ukraine;) was preliminary calcined during 2 h at 400 °C by heating on air in order remove any organic substances. *O*-{(4-tert-butylcyclohexyl)-2-acetamido-2,3-dideoxy-β-d-glucopyranoside-3-yl}-*D*-lactoyl-*L*-alanyl-*D*-isoglutamine (MDP *O*-glycoside , the scheme 1) was kindly gifted by the Department of Biological and Organic chemistry of Taurida National V.I. Vernadsky University [40, 41]. Sample of MDP *O*-glycoside with a concentration of 0.6 mmol/g of on the silica surface was obtained by impregnation.

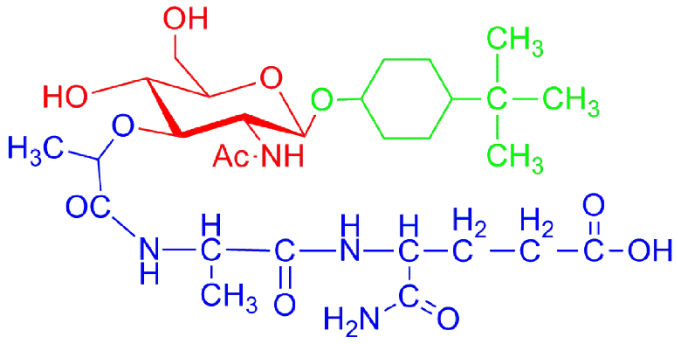


**Scheme 1.** Structure of MDP *O*-glycoside

Soaking of 1 g of silica in the 20 mL of 96% ethanol solution containing 0.378 g of MDP *O*-glycoside used for obtaining sample of MDP *O*-glycoside adsorbed on the silica surface with a concentration of 0.6 mmol/g of on the silica surface. This concentration was selected in order to cover all isolated silanol groups (the main active cites) on the silica surface. The

thoroughly mixed suspension of modifier and silica left on air at ~20 °C for full evaporation of the ethanol (~ 24 h). Thereafter, the sample of MDP *O*-glycoside adsorbed on the silica was studied by TPD-MS and FT-IR-spectroscopy.

Method of Temperature-Programmed Desorption Mass Spectrometry (TPD-MS). TPD-curves for MDP *O*-glycoside in pristine state and on the silica surface were received by MKh-7304A monopole mass spectrometer (Electron, Sumy, Ukraine) with electron impact ionization. The detail description of experimental work and calculation of kinetic parameters were reported in previous articles [42-47].

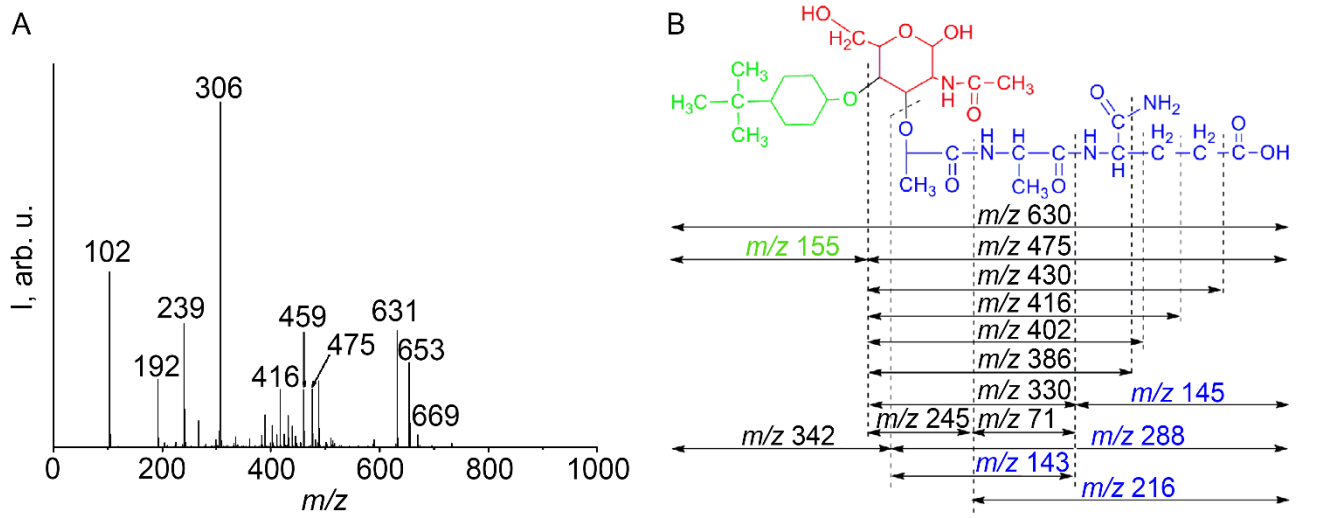


***Figure 1.*** (A) ESI-MS spectrum of MDP *O*-glycoside in positive mode; (B) Fragmentation pattern of MDP *O*-glycoside under ESI-MS investigation.

*FTIR Spectroscopy.* FT IR NEXUS spectrometer was used for obtaining FT-IR-spectra (Thermo Nicolet). FT-IR spectra were run in diffuse reflection mode at a resolution of 4 $cm^{-1}$in the frequency range of 4000–400 $cm^{-1}$at room temperature, and scan rate 0.5 cm/sec. The milled MDP *O*-glycoside adsorbed on the silica sample were mixed thoroughly with preliminary calcined and milled KBr (1:100).

Electrospray mass spectrometry (ESI-MS). Bruker HCT Plus (Bruker Daltonics, Bremen, Germany) equipped with an electrospray ionization source with an ion trap mass spectrometer was used to obtain ESI mass spectra at 25°C. A 250 pmol/μL of the analyte methanol solution was used for the analysis.

*RESULTS*

It was reported that MDP structure consists of two type adjacent β-turns held in S-shaped structure. Biological activity depends on spatial organization of their molecules. Binding some functional groups of molecules to active site of carrier can change or totally illuminate their activity. Silica is commonly used as vehicles for bioactive agents in different drug delivery systems. Currently, researchers across the globe are developing less pyrogenic analogues of MDP that retain their biological activity. Parfenyuk and co-authors showed that MDP derivative, glucosaminylmuramyl dipeptide (GMDP), lost his biological effect after immobilization on unmodified silica surface. Obviously, there is an inactivation occurs due to interaction between silica surface active sites and GMDP groups responsible for its pharmacological activity. Therefore, understanding the structure-biological activity relationship is important for the creation of new derivatives of MDP as well as for design drug delivery systems based on them.

A demand arose for confirming structure and stability during storage of MDP *O*-glycoside as it was synthesized. Moreover, ion-molecule reactions of molecular ion can in some extend model the reaction pathways of thermally stimulated reactions as well as biotransformation pathways of MDP in the natural conditions. Chemical structure and stability of MDP *O*-glycoside during storage have been confirmed by electrospray mass spectrometry (Figure 1) and $^1$H-NMR [41].

In spectrum we can see peaks at *m/z* 653, 631, which correspond to sodium $\left[M + Na\right]^+$ and proton $\left[M + H\right]^+$ molecular ion adducts, respectively (Figure 1). Moreover, there is spectrum low-intensity peak at *m/z* 669, which is belongs to potassium molecular ion adduct $\left[M + K\right]^+$. Ion peak at *m/z* 475 formed under glycosidic linkage cleavage. The elimination of $NH_2$ from ion at *m/z* 475 lead to ion peak at *m/z* 459. Ion peak at *m/z* 416 is resulting from detachment of $-CH_2-COOH$ fragment from ion at *m/z* 475 (Figure 1B). Ion peaks at *m/z* 239 and at *m/z* 192 are triple-charged $\left[M + K + 2Na\right]^{3+}/_3$ and quadro-charged

$[M - 6H + 6Na + 4H]^{4+}/_{4}$ adducts, respectively. The loss of two water molecule from the ion at *m/z* 342 led to the formation of the peak ion at *m/z* 306. Peak ion at *m/z* 102 is a triple-charged ion at *m/z* 306 $[M - C_{11}H_{18}N_3O_6 - 2H_2O]^{3+}/_{3}$. All fragment ions in ESI MS spectra of MDP are coincided with the structure of MDP *O*-glycoside.

The TPD-MS is frequently employed technique to monitor surface interactions between adsorbed molecules and substrate surface. The TPD-MS can be used for the determination of kinetic and thermodynamic parameters of desorption processes or decomposition reactions. It can be recognized the binding states of the adsorbed species and surface sites responsible for a given surface thermal transformation. Pyrolysis of carbohydrate fragment, aglycone and peptide fragment of MDP *O*-glycoside in the pristine state and adsorbed on the silica surface (Figure 2-4) have been determined by TPD-MS. Earlier we identified pyrolysis stages of MDP *O*-glycoside in the pristine state and adsorbed on silica surface [40]. Our study has revealed that binding of MDP *O*-glycoside to silica surface occurs by means of peptide fragment but detailed investigation of binding mechanism haven`t done yet. Briefly, the pyrolysis of MDP *O*-glycoside at the pristine state occurs at two stages (Figures 2-4). The first stage relates to the simultaneous detachment of peptide fragment (*m/z* 99, 79, 77, 71) and aglycone (*m/z* 138, 82) from pyranose ring of muramic acid (Figures 2, 4). Peak ions at *m/z* 79, 77 were detected during analysis of TPD spectra (Figure 4 D, E). But structure of these ions haven`t been elucidated in our previous work. Apart from peak ions at *m/z* 79, 77 observed on TPD-curves of MDP *O*-glycoside adsorbed on silica surface as it was detected in pristine state additional ion at *m/z* 108 (Figure 4C) have been revealed. Fragment ions at *m/z* 108, 79, 77, 51 ($T_{max}$=80 °C) are derived from peptide fragment of MDP *O*-glycoside (Figure 3C-F).

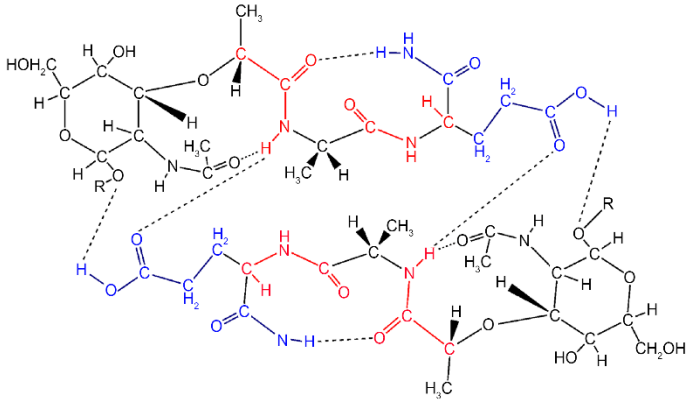

***Scheme 2.*** *Complex of MDP O-*glycoside *in the pristine state under TPD-MS investigation.*

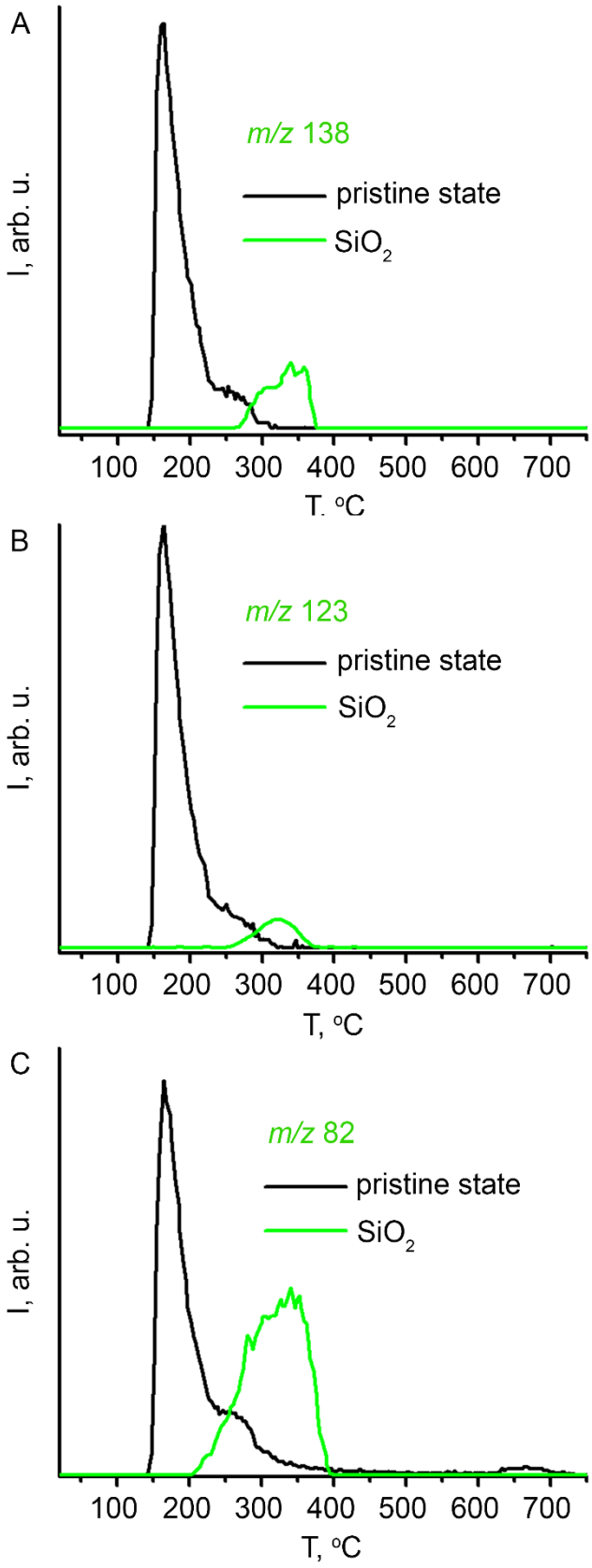


***Figure 2.*** TPD-curves of aglycone decomposition. (A) TPD-curves of fragment ion (*m/z* 138) desorption for the samples of MDP *O*-glycoside in pristine state (black curve) and on the silica surface (green curve); (B) TPD-curves of fragment ion (*m/z* 123) desorption for the samples of MDP *O*-glycoside in pristine state (black curve) and on the silica surface (green curve); (C) TPD-curves of fragment ion (*m/z* 82) desorption for the samples of MDP *O*-glycoside in pristine state (black curve) and on the silica surface (green curve).

Presumably, removal of peptide fragment and aglycon from muramic acid in the pristine state arise due to glycoside bonds cleavage during one thermal reaction ($T_{max}$=160 °C). In this case, intermolecular catalysis takes place. Elimination of peptide fragment from one molecule triggers the removal of the aglycone from neighbor molecule (scheme 2). This causes the second order of reaction [40]. Both substituents have values of pre-exponential factor of the same order. Activation energies have close values approximately 132 kJ/mole [40].

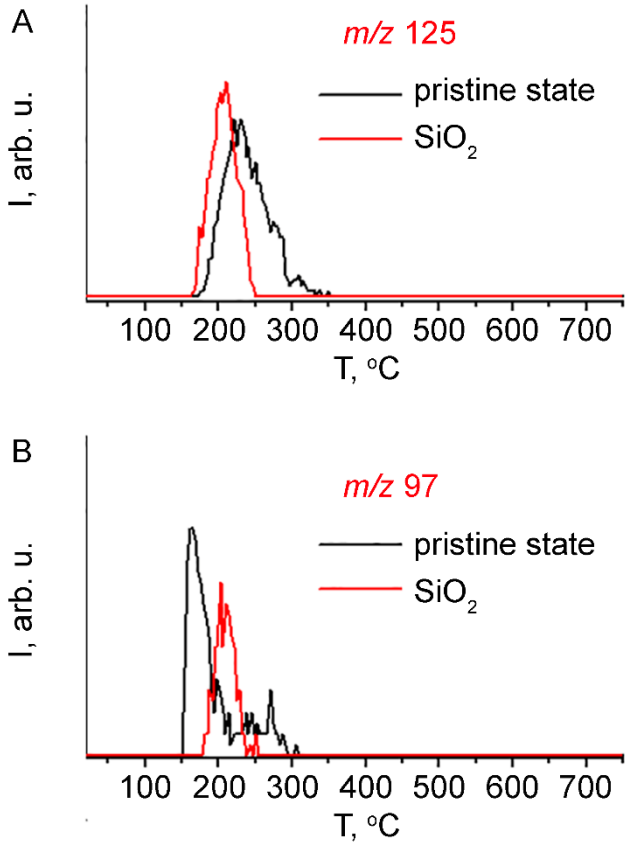


***Figure 3.*** TPD-curves of carbohydrate fragment decomposition. (A) TPD-curves of unsaturated aminosugar (*m/z* 125) desorption for the samples of MDP *O*-glycoside in pristine state (black curve) and on the silica surface (red curve); (B) TPD-curves of fragment ion (*m/z* 97) desorption for the samples of MDP *O*-glycoside in pristine state (black curve) and on the silica surface (red curve).

The pyrolysis of carbohydrate fragment in the pristine state and on the silica surface takes place at ≈250 °C due to glycosidic linkage disruption and elimination of two water molecules from pyranose ring of MDP *O*-glycoside with formation of substance in molecular form with *m/z* 125 (Figure 3A). This reaction both in pristine state and on the silica surface follows first order kinetics.

It was found that the thermal decomposition of MDP *O*-glycoside on the silica surface proceeds in three stages (Figure 2-4). Thermal decomposition of aglycone and peptide fragment on the silica surface proceeds via another mechanism, then transformations of carbohydrate fragment. The decomposition of peptide fragment and aglycone on the silica surface occurs as two different reactions in various temperature ranges and characterized by distinct kinetic parameters of reactions (Figure 2, 4). Most probably, the decomposition of aglycone (Figure 2) and peptide fragment (Figure 4) of MDP *O*-glycoside on the silica surface takes place via breaking of hydrogen-bonded complex at silanol surface group. Formation on the surface of adsorption complexes between MDP *O*-glycoside molecule and silanol group of the surface and the absence attractive or cooperative interactions between molecules of adsorbate supports differences in pyrolytic pathways of MDP *O*-glycoside on the surface and in the pristine state. Nearest environment plays a decisive role at pyrolysis in the pristine state.

The calculated kinetic parameters for fragments at *m/z* 108, 79 indicate that process follows first order kinetics (Table 1) as previously was calculated for peptide fragment pyrolysis on the silica surface. Further TPD-MS data analysis were undertaken in order to identify structure of ions at *m/z* 79, 77, which previously weren`t known.

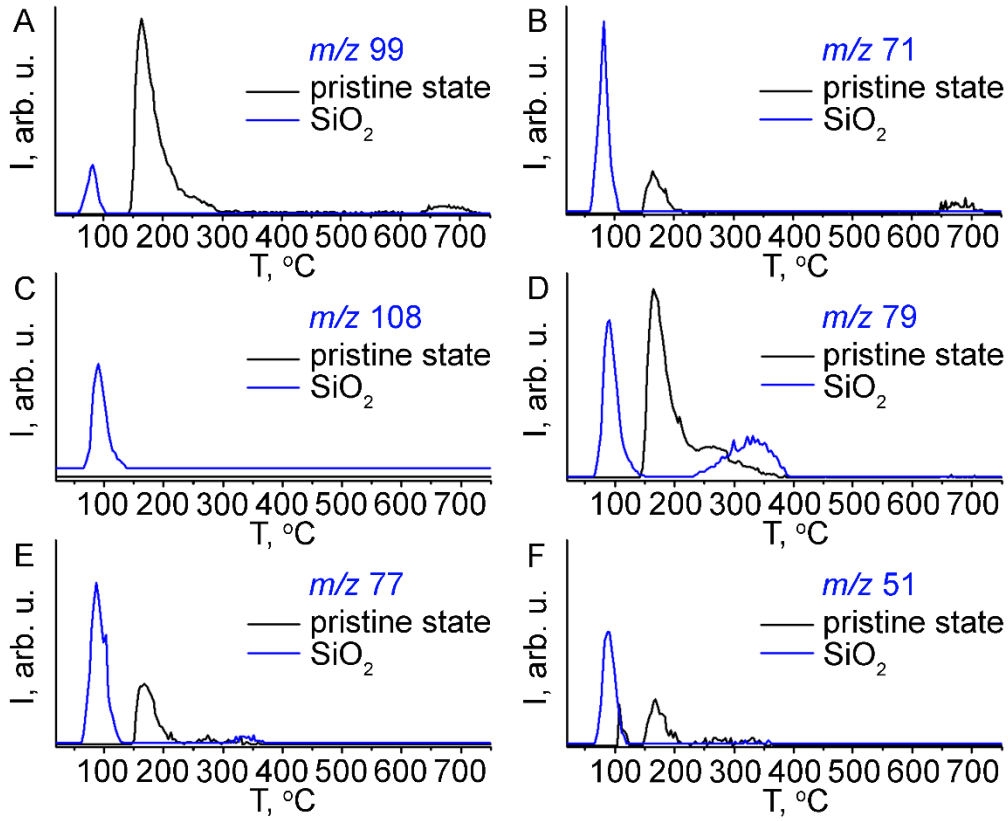


***Figure 4.*** TPD-curves of peptide fragment decomposition. (A) TPD-curves of fragment ion (*m/z* 99) desorption for the samples of MDP *O*-glycoside in pristine state (black curve) and on the silica surface (blue curve); (B) TPD-curves of fragment ion (*m/z* 71) desorption for the samples of MDP *O*-glycoside in pristine state (black curve) and on the silica surface (blue curve); (C) TPD-curves of fragment ion (*m/z* 108) desorption for the samples of MDP *O*-glycoside in pristine state (black curve) and on the silica surface (blue curve) (D) TPD-curves of fragment ion (*m/z* 79) desorption for the samples of MDP *O*-glycoside in pristine state (black curve) and on the silica surface (blue curve); (E) TPD-curves of fragment ion (*m/z* 77) desorption for the samples of MDP *O*-glycoside in pristine state (black curve) and on the silica surface (blue curve); (F) TPD-curves of fragment ion (*m/z* 51) desorption for the samples of MDP *O*-glycoside in pristine state (black curve) and on the silica surface (blue curve).

Table 1. Kinetic parameters (temperature of the maximum reaction rate $T_{max}$, reaction order $n$, activation energy $E^{\neq}$, pre-exponential factor $k_0$, change in activation entropy $\Delta S^{\neq}$) of thermal transformations of MDP in pristine and adsorbed on silica surface state

| **Fragment** | **$T_{max}$ (°C)** | ***m/z*** | **n** | **$E^{\neq}$, (kJ×mol$^{-1}$)** | **$k_0$, (s$^{-1}$ )** | **$\Delta S^{\neq}$, (cal×K$^{-1}$×mol$^{-1}$)** | **$R^2$** |
|---|---|---|---|---|---|---|---|
| *Adsorbed state* | | | | | | | |
| *peptide fragment* | *3-iminopyridine-2(3H)-one* | | | | | | |
| | *90* | *108* | *1* | *72* | *$2.6\times10^8$* | *-20* | *0.950* |
| | *90* | *79* | *1* | *75* | *$9.0\times10^8$* | *-18* | *0.963* |

The IR-spectroscopy data of MDP *O*-glycoside investigations in the pristine state and adsorbed on the silica surface are in a good agreement with the TPD-data (Figure 4). FTIR spectrum of silica is illustrated on Fig. 5A (curve 2, black line). The narrow band at 3745 cm$^{-1}$ is assigned to the stretching mode of isolated silanol groups (Figure 5A, curve 2 (black curve), 3 (blue curve)). The wide absorption band between 3000 and 3700 cm$^{-1}$ corresponds to overlapping of water O–H and Si–OH stretching vibrations. Absorption bands at 1980 cm$^{-1}$, 1867 cm$^{-1}$ characterize the overtones and combination modes of the silica matrix. The peak at 1624 cm$^{-1}$ is attributed to the bending vibrations of physically adsorbed molecular water at the silica surface (Figure 5A, curve 2). The intense band at ~1083 cm$^{-1}$ and the shoulder at ~1197 cm$^{-1}$ associated with the asymmetric Si–O–Si

stretching vibrations (the transversal optical and longitudinal optical modes, respectively or assigned to asymmetric stretching vibrations of the Si-O-Si. The band at ~806 $cm^{-1}$ caused by symmetric Si–O–Si vibrations.

FT-IR spectra of MDP *O*-glycoside in pristine state exhibit bands in the range 4000–3100 $cm^{-1}$ resulting from the O–H stretching bands and the symmetric and asymmetric N–H stretching modes. IR spectra of MDP *O*-glycoside adsorbed on the silica surface in the range 4000–3100 $cm^{-1}$ are also dominated by absorption arising from –OH and N–H stretching mode, which are partially overlapped by the bands of the silica matrix (Figure 5A).

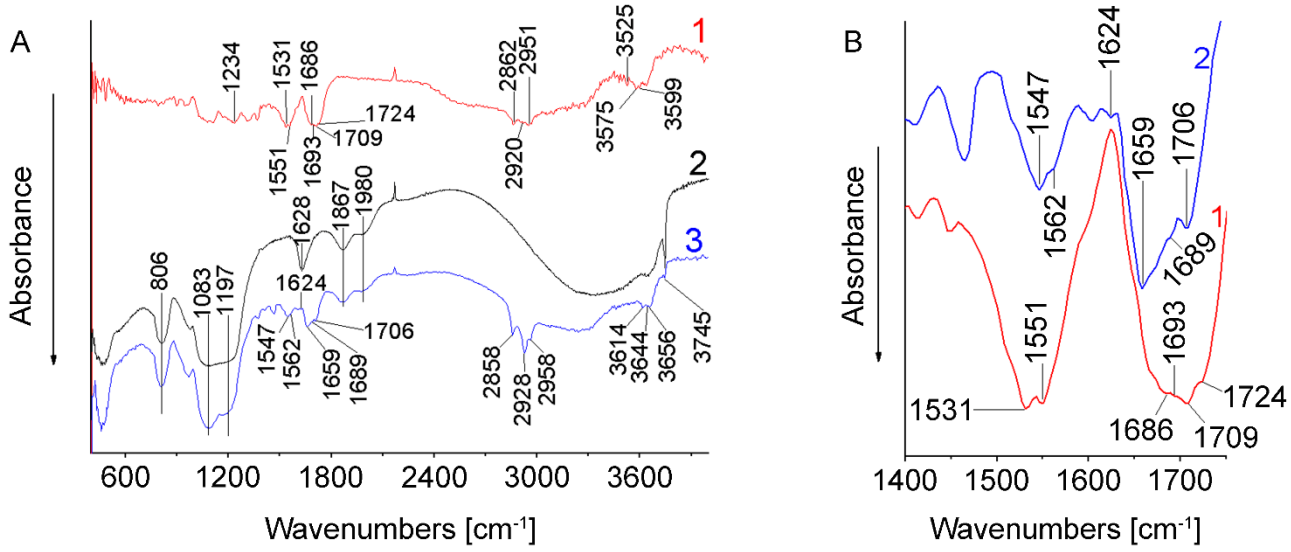


**Figure 5.** (A) FTIR spectra from MDP *O*-glycoside (1; red line), fumed silica (2; black line) and MDP *O*-glycoside immobilized on the silica surface (0.6 mmol/g) (3; blue line); (B) FTIR spectra in the range between 1400 and 1800 $cm^{-1}$ from MDP *O*-glycoside (1; red line) and MDP *O*-glycoside immobilized on the silica surface (0.6 mmol/g) (2; blue line).

Table 2. Absorption frequencies of amide I, amide II bands and N–H stretching modes of MDP in pristine state (Pr) and andorbed on silica surface (Ad)

| | **Amide I, ν ($cm^{-1}$)** | | **Amide II, ν ($cm^{-1}$)** | | **$\nu_{N-H}$, ($cm^{-1}$)** | |
|---|---|---|---|---|---|---|
| | **Pr** | **Ad** | **Pr** | **Ad** | **Pr** | **Ad** |
| MDP | 1686<br>1693 | 1659<br>1689 | 1531<br>1551 | 1547<br>1562 | 3525<br>3575<br>3599 | 3614<br>3644<br>3656 |

Table 3. The amide I, amide II bands frequencies and assignments to the secondary structure of peptides and proteins (according to literature)

| **Assignment** | **Amide I, ν ($cm^{-1}$)** | **Amide II, ν ($cm^{-1}$)** | **Reference** |
|---|---|---|---|
| α-helix | 1663<br>1660-1662,1665<br>1650-1658 | 1537<br>1531-1533<br>- | [48, 49]<br>[50]<br>[51] |
| β-sheet | 1670-1690, 1620-1640<br>1620-1640 | -<br>- | [50]<br>[51] |

| | | | |
|---|---|---|---|
| β-turn | 1659; 1686; 1689; 1693<br>1659, 1686, 1689, 1693<br>1660-1690, 1635-1645, 1693, 1659 | 1531; 1547, 1562<br>1531, 1551, 1547<br>- | [52]<br>[49]<br>[50] |
| random coil | 1640-1648, 1650-1660 | - | [50] |

The stretching vibrations of terminal silanol groups of silica appeared at 3745 $cm^{-1}$ in IR-spectra. The intensity of band at 3745 $cm^{-1}$ is decreased after immobilization of MDP on the silica surface. That fact indicates on the hydrogen-bonding of MDP molecule with free silanol surface groups.

In the IR-spectrum of MDP *O*-glycoside in the pristine state, the lines at 2862 and 2920 $cm^{-1}$ are attributed to the symmetric and antisymmetric stretching vibrations of C−H bonds in a methylene group. At the same time in the IR-spectrum of MDP *O*-glycoside on the silica surface the lines at 2858 $cm^{-1}$ and 2928 $cm^{-1}$ is also caused by the symmetric and antisymmetric stretching vibrations of C−H bonds in a methylene group.

Bands at 1709 $cm^{-1}$ (dimer of carboxylic group) and 1724 $cm^{-1}$ (hydrogen-bonded carboxylic group, associated carboxylic group) referred to stretching vibrations of C=O bonds in carbonyl group. Detected shift of these bands to lower wavenumbers (1709 $cm^{-1}$) provide evidence for surface complex formed by C=O of MDP *O*-glycoside carbonyl group (Figure 5, Table 2). The bands observed in the 1500–1200 $cm^{-1}$ region arise from deformation vibrations. Amide III band at 1234 $cm^{-1}$ that derives from deformation vibrations of N−H bond, wasn`t detected in IR-spectrum of MDP *O*-glycoside on the silica surface. Region 1400–1200 $cm^{-1}$ are characterized by overlapping deformation vibrations of C–H bond in methyl and methylene groups of peptide fragment, stretching vibrations of C-O bond in carbonyl group, deformation vibrations of O−H bond in hydroxyl group and stretching vibrations of C–N bond. The region between 1800 and 1500 $см^{-1}$ is dominated by the conformational-sensitive amide I and amide II bands, which are the most intensive bands in the spectra of MDP *O*-glycoside in pristine and adsorbed state. Amide I is mainly induced by the stretching vibrations of the C=O of peptide bond and describes vibration produces a change of C=O bond length, that encodes the secondary structure of a protein [38, 39]. The amide I band contour have a complex composite because it consists of many overlapping component bands representing alpha helices, β-sheets, β-turns and random structures. Amide I band of MDP *O*-glycoside in pristine state is consists of two separate component peaks at 1686 and 1693 $cm^{-1}$ (Figure 5B). It indicates that MDP *O*-glycoside molecule has unequal C=O bonds [53-55]. The peaks at 1659 and 1689 $cm^{-1}$ in the spectra of MDP *O*-glycoside adsorbed on silica are related to the amide I band (Figure 5B, Table 2); hence it is observed that amide I band is shifted to lower wavenumbers (Figure 5B, Table 2). This testify that binding to the silica surface occur due to peptide fragment resulting in changing of its conformation under adsorption. The amide II band represents mainly the out-of-phase combination of the N−H in-plane bend and the C–N stretching vibration. Amide II band of MDP *O*-glycoside in pristine state shows also a complex structure: 1531, 1551 $cm^{-1}$ and on the silica surface: 1547, 1562 $cm^{-1}$, respectively [53-55] (Figure 5B, Table 2).

The physically adsorbed molecular water at the silica surface give absorbance band at 1624 $cm^{-1}$ (Figure 5A, curve 3). Hence, amide I and amide II bands are not obscured by overlapping with absorption bands of physically adsorbed molecular water.

As it was mentioned above, earlier other researchers on the basis of NMR data found that MDP appears in an S-shaped structure composed of two adjacent type II β-turns [30-32]. β-turns are peptide and protein secondary structural element which formation plays an important role in protein folding, protein stability and molecular recognition processes.

In FTIR-spectra β-turns give rise to certain absorption bands namely, amide I and partially amide II [38] (Table 3). Amide I and amide II are sensitive to the secondary structure content of a peptide or protein because peptide bonds are involved in the hydrogen bonding that takes place between the different elements of secondary structure[56]. Assignment of amide I has revealed that peptide fragment of MDP *O*-glycoside formed by two type II β-turns in pristine and immobilized on silica surface state.

Amide I band in IR-spectra of MDP *O*-glycoside immobilized on the silica surface is shifted to lower wavenumbers however it keeps at the same time the complex structure of the spectral line, which can be assigned to β-turns. First β-turn is due to hydrogen bonding between C=O bond of acetamido group of *N*-acetylmuramic acid and N−H bond of alanine. Second β-turn involving hydrogen bonds between carbonyl group of the lactyl side-chain of *N*-acetylmuramic acid and $NH_2$ group of isoglutamine. Therefore, amide I and amide II bands in IR-spectra of MDP *O*-glycoside in the pristine state and adsorbed on the silica surface have complex structure: include several lines. Amide band frequency splitting indicates that amide groups participate in the formation of energetically unequal hydrogen bonds. As it was mentioned above, amide II band is shifted to a higher wavenumbers and amide I band is shifted to a lower wavenumber in IR-spectra of MDP *O*-glycoside adsorbed on the silica surface, which testify that MDP *O*-glycoside binds to surface by means of carboxyl group of isoglutamine and one of peptide groups (Figure 5, Table 2). Adsorption of MDP *O*-glycoside on the silica surface resulted in conformational changes of MDP *O*-glycoside molecule.

FTIR and TPD-MS data of MDP *O*-glycoside in pristine and immobilized on silica surface states that MDP *O*-glycoside binds to the silica surface by means of carboxylic and NH moieties of isoglutamine (the scheme 3). Moreover, pyrolysis of

MDP *O*-glycoside on the silica surface proceeds through formation of additional product 3-iminopyridine-2(3H)-one, which identified in mass spectra as molecular ion with *m/z* 108 and its fragment ions with *m/z* 79, 77, 51 (the scheme 3).

SUMMARY

Investigation of MDP *O*-glycoside conformation in pristine state and immobilized on the surface is important for understanding of interactions of biomolecules with different receptors on cell membranes, as glycopeptides include the enzymes, hormones, immune and plasma proteins. Since MDP *O*-glycoside is a conformationally flexible molecule, its various biological activities could be due to interactions of different conformations with stereochemically different receptors.

FTIR and TPD-MS data confirm existence of a MDP *O*-glycoside first β-turn on the silica surface resulting from the formation of a hydrogen bond between the NAc carbonyl and the *L*-Ala NH for MDP *O*-glycoside and its analogs, as reported previously. It can be supposed that MDP *O*-glycoside don`t lose its immunostimulating activity after immobilization on silica surface as previously a relationship between the expression of such a biological activity and the existence of the first turn has been suggested. Formation on the surface of adsorption complexes between MDP *O*-glycoside molecule and silanol group of the surface causes differences in pyrolytic pathways of MDP *O*-glycoside on the surface and in the pristine state. Using TPD-MS and FTIR-spectroscopy has been shown that adsorption of MDP *O*-glycoside on silica surface takes place via carboxylic group and –NH group of isoglutamine, not involved in hydrogen-bonded β-turns. The results demonstrate that TPD-MS and FTIR-spectroscopy may be applied to study conformation of MDP.

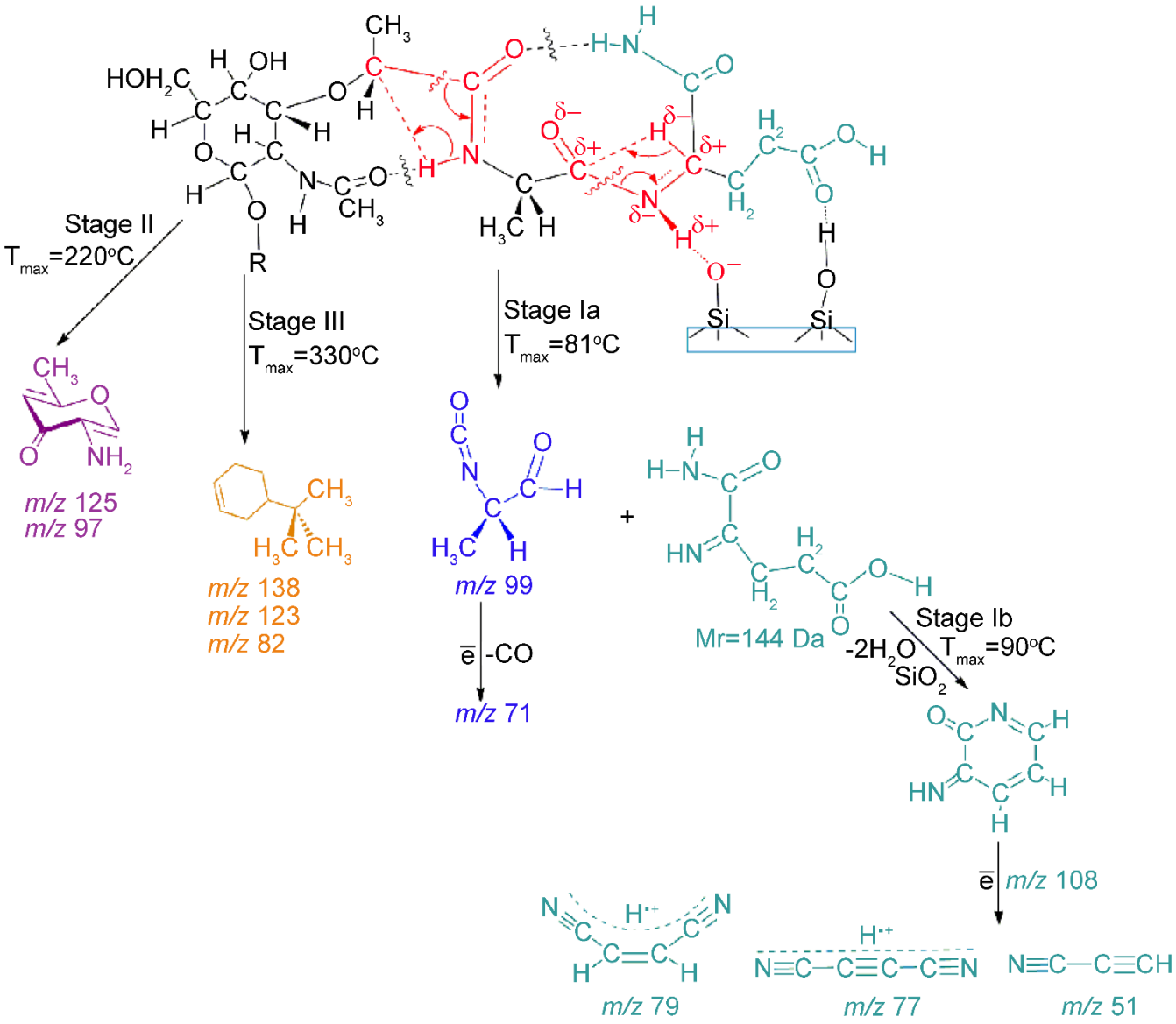


**Scheme 3.** Decomposition pathway of MDP *O*-glycoside on the silica surface under TPD-MS investigation.

**Author information**

**Corresponding Author**

*E-mail: liana.azizova@yahoo.com
Dr. Tetiana Kulik tanyakulyk@i.ua

**Author Contributions**

*These authors contributed equally to this work.
The last version of the manuscript was approved by all authors. The authors state that this article is unique, has not been published and isn't under consideration for publication somewhere else. The authors confirm that there is no conflict of interest.

**Funding Sources**

This publication is based on work supported by the grant FSA3-20-66700 from the U.S. Civilian Research & Development Foundation (CRDF Global) with funding from the United States Department of State. Liana Azizova thanks for financial support from the Horizon 2020 DualFun project (H2020-MSCA-IF-2016, grant agreement No. 749207).

**Acknowledgment**

The authors express their sincere gratitude to Dr. Howard Dodd for technical assistance with the ESI-MS measurements. The authors express their thanks to Professor Alexander Zemlyakov and Dr. Viktoriya Tsikalova for providing the synthesized sample of MDP *O*-glycoside.

**Abbreviations**

MDP muramyl dipeptide; TPD-MS temperature programmed desorption mass spectrometry; FTIR fourier transform infrared spectroscopy; ESI MS electrospray mass spectrometry; NMR nuclear magnetic resonance.

**References**

[1] M.R. Pratt, C.R. Bertozzi, Synthetic glycopeptides and glycoproteins as tools for biology, Chemical Society Reviews, 34 (2005) 58-68.
[2] F. Ellouz, A. Adam, R. Ciorbaru, E. Lederer, Minimal structural requirements for adjuvant activity of bacterial peptidoglycan derivatives, Biochemical and Biophysical Research Communications, 59 (1974) 1317-1325.
[3] P. Lefrancier, J. Choay, M. Derrien, I. Lederman, Synthesis of *N*-acetyl-muramyl-*L*-alanyl-*D*-isoglutamine, an adjuvant of the immune response, and of some *N*-acetyl-muramyl-peptide analogs, International Journal of Peptide and Protein Research, 9 (1977) 249-257.
[4] S.E. Girardin, L.H. Travassos, M. Herve, D. Blanot, I.G. Boneca, D.J. Philpott, P.J. Sansonetti, D. Mengin-Lecreulx, Peptidoglycan Molecular Requirements Allowing Detection

by Nod1 and Nod2, J. Biol. Chem., 278 (2003) 41702–41708.
[5] Z. Liang , H. Zhu, X. Wang, B. Jing, Z. Li, X. Xia, H. Sun, Y. Yang, W. Zhang, L. Shi, H. Zeng, B. Sun, Adjuvants for Coronavirus Vaccines, Frontiers in Immunology, 11 (2020).
[6] C. Poon, A.A. Patel, Organic and inorganic nanoparticle vaccines for prevention of infectious diseases, Nano Express, 1 (2020) 012001.
[7] D. Yang, Application of Nanotechnology in the COVID-19 Pandemic, Int. J. Nanomedicine, 16 (2021) 623-649.
[8] A.T. Yayehrad, E.A. Siraj, G.B. Birhanu, A.A. Alemie, M.T. Derseh, A.S. Ambaye, Could Nanotechnology Help to End the Fight Against COVID-19? Review of Current Findings, Challenges and Future Perspectives Int. J. Nanomedicine. , 16 (2021) 5713-5743.

[9] V.M. Gun'ko, I.F. Mironyuk, V.I. Zarko, E.F. Voronin, V.V. Turov, E.M. Pakhlov, E.V. Goncharuk, Y.M. Nychiporuk, N.N. Vlasova, P.P. Gorbik, O.A. Mishchuk, A.A. Chuiko, T.V. Kulik, B.B. Palyanytsya, S.V. Pakhovchishin, J. Skubiszewska-Zięba, W. Janusz, A.V. Turov, R. Leboda, Morphology and surface properties of fumed silicas, Journal of Colloid and Interface Science, 289 (2005) 427-445.
[10] L.F. Sharanda, A.P. Shimansky, T.V. Kulik, A.A. Chuiko, Study of acid-base surface properties of pyrogenic γ-aluminium oxide, Colloids and Surfaces A: Physicochemical and Engineering Aspects, 105 (1995) 167-172.
[11] D.H.M. Buchold, C. Feldmann, Nanoscale γ-AlO(OH) Hollow Spheres: Synthesis and Container-Type Functionality, Nano Letters, 7 (2007) 3489-3492.
[12] J. Conde, J.T. Dias, V. Grazú, M. Moros, P.V. Baptista, J.M. de la Fuente, Revisiting 30 years of biofunctionalization and surface chemistry of inorganic nanoparticles for nanomedicine, Frontiers in Chemistry, 2 (2014).
[13] F. Dilnawaz, Multifunctional Mesoporous Silica Nanoparticles for Cancer Therapy and Imaging, Current Medicinal Chemistry, 26 (2019) 5745 - 5763.
[14] J.J. Giner-Casares, M. Henriksen-Lacey, M. Coronado-Puchau, L.M. Liz-Marzán, Inorganic nanoparticles for biomedicine: where materials scientists meet medical research, Materials Today, 19 (2016) 19-28.

[15] T. Ruhland, S.D. Nielsen, P. Holm, C.H. Christensen, Nanoporous Magnesium Aluminometasilicate Tablets for Precise, Controlled, and Continuous Dosing of Chemical Reagents and Catalysts: Applications in Parallel Solution-Phase Synthesis, Journal of Combinatorial Chemistry, 9 (2007) 301-305.
[16] M. Kaurav, J. Madan, M.S. Sudheesh, R.S. Pandey, Combined adjuvant-delivery system for new generation vaccine antigens: alliance has its own advantage, Artificial Cells, Nanomedicine, and Biotechnology, 46 (2018) S818-S831.
[17] N. Chauhan, S. Tiwari, T. Iype, U. Jain, An overview of adjuvants utilized in prophylactic vaccine formulation as immunomodulators, Expert Review of Vaccines, 16 (2017) 491-502.
[18] C. Barbé, J. Bartlett, L. Kong, K. Finnie, H.Q. Lin, M. Larkin, S. Calleja, A. Bush, G. Calleja, Silica Particles: A Novel Drug-Delivery System, Advanced Materials, 16 (2004) 1959-1966.
[19] H. Chen, Y. Wang, S. Dong, E. Wang, Direct Electrochemistry of Cytochrome c at Gold Electrode Modified with Fumed Silica, Electroanalysis, 17 (2005) 1801-1805.
[20] G.A.M. Mersal, M. Khodari, U. Bilitewski, Optimisation of the composition of a screen-printed acrylate polymer enzyme layer with respect to an improved selectivity and stability of enzyme electrodes, Biosensors and Bioelectronics, 20 (2004) 305-314.
[21] J.M. Rosenholm, A. Meinander, E. Peuhu, R. Niemi, J.E. Eriksson, C. Sahlgren, M. Lindén, Targeting of Porous Hybrid Silica Nanoparticles to Cancer Cells, ACS Nano, 3 (2008) 197-206.
[22] I.I. Slowing, B.G. Trewyn, S. Giri, V.S. Lin, Mesoporous Silica Nanoparticles for Drug Delivery and Biosensing Applications, Advanced Functional Materials, 17 (2007) 1225-1236.
[23] B.G. Trewyn, I.I. Slowing, S. Giri, H.-T. Chen, V.S.Y. Lin, Synthesis and Functionalization of a Mesoporous Silica Nanoparticle Based on the Sol–Gel Process and Applications in Controlled Release, Accounts of Chemical Research, 40 (2007) 846-853.
[24] J. Wang, J. Liu, Fumed-silica containing carbon-paste dehydrogenase biosensors, Analytica Chimica Acta, 284 (1993) 385-391.
[25] E.V. Parfenyuk, N. Alyoshina, Y.S. Antsiferova, N.Y. Sotnikova, Silica Nanoparticles as Drug Delivery System for Immunomodulator Gmdp, American Society of Mechanical Engineers2012.
[26] B.M. Chapman B.E., Redmond J.W., Proton N.M.R. of the muramyl dipeptide adjuvant in dimethyl sulfoxide, Australian Journal of Chemistry, 35 (1982) 489-493.
[27] T.D.J. Halls, M.S. Raju, E. Wenkert, M. Zuber, P. Lefrancier, E. Lederer, The anomeric configuration of the immunostimulant N-acetylmuramoyl-dipeptide and some of its derivatives, Carbohydrate Research, 81 (1980) 173-176.
[28] E.F. Mcfarlane, C. Martinic, 400-MHz H N.M.R. of adjuvant muramyl dipeptide in dimethyl sulfoxide, Australian Journal of Chemistry, 36 (1983) 1087-1096.
[29] H. Okumura, I. Azuma, M. Kiso, A. Hasegawa, The equilibrium compositions and conformations of some carbohydrate analogs of *N*-acetylmuramoyl-*L*-alanyl-*D*-isoglutamine as determined by $^{1}$H-N.M.R. spectroscopy, Carbohydrate Research, 117 (1983) 298-303.
[30] S. Fermandjian, B. Perly, M. Level, P. Lefrancier, A comparative $^{1}$H-N.M.R. study of MurNAc-*L*-Ala-*D*-iGln (MDP) and its analogue murabutide: Evidence for a structure involving two successive β-turns in MDP, Carbohydrate Research, 162 (1987) 23-32.
[31] P. Sizun, B. Perly, M. Level, P. Lefrancier, S. Fermandjian, Solution conformations of the immunomodulator muramyl peptides, Tetrahedron, 44 (1988) 991-997.
[32] Y. Boulanger, Y. Tu, V. Ratovelomanana, E. Purisima, S. Hanessian, Conformation of MurNAc-*L*-Ala-*D*-iGln (MDP) and of a constrained analog using $^{1}$H NMR data and molecular modeling, Tetrahedron, 48 (1992) 8855-8868.
[33] V. Harb, J. Mavri, J. Kidric, D. Hadzi, Solution conformation of the immunomodulator muramyl dipeptide : restrained molecular dynamics based on nuclear magnetic resonance data and semiempirical MO study, Croatica chemica acta, 64 (1991) 551-559.
[34] P. Pristovšek, J. Kidrič, J. Mavri, D. HadžI, NMR and molecular dynamics study of four carbocyclic muramyl dipeptide analogues, Biopolymers, 33 (1993) 1149-1157.
[35] A.T. Hubbard, The Handbook of Surface Imaging and Visualization, CRC PressINC1995.
[36] S.I. Nicholl, J.W. Talley, Development of thermal programmed desorption mass spectrometry methods for environmental applications, Chemosphere, 63 (2006) 132-141.
[37] D.P. Woodruff, T.A. Delchar, Modern Techniques of Surface Science, Cambridge University Press1994.
[38] A. Barth, P.I. Haris, Biological and Biomedical Infrared Spectroscopy, Ios PressInc 2009.
[39] P.I. Haris, D. Chapman, The conformational analysis of peptides using fourier transform IR spectroscopy, Biopolymers, 37 (1995) 251-263.
[40] T.V. Kulik, L.R. Azizova, B.B. Palyanytsya, A.E. Zemlyakov, V.N. Tsikalova, Mass spectrometric investigation of synthetic glycoside of muramyl dipeptide immobilized on fumed silica surface, Materials Science and Engineering: B, 169 (2010) 114-118.
[41] A. Zemlyakov, V. Tsikalova, V. Tsikalov, V. Chirva, E. Mulik, O. Kalyuzhin, Synthesis and Protective Activity of β-Glycosides of of *N*-Acetylmuramyl-*L*-Alanyl-*D*-Isoglutamine with Alkylalicyclic and Arylaliphatic Aglycons, Russian Journal of Bioorganic Chemistry, 31 (2005) 576-582.
[42] T.V. Kulik, Use of TPD–MS and Linear Free Energy Relationships for Assessing the Reactivity of Aliphatic Carboxylic Acids on a Silica Surface, The Journal of Physical Chemistry C, 116 (2011) 570-580.

[43] K. Kulyk, V. Ishchenko, B. Palyanytsya, V. Khylya, M. Borysenko, T. Kulyk, A TPD-MS study of the interaction of coumarins and their heterocyclic derivatives with a surface of fumed silica and nanosized oxides CeO2/SiO2, TiO2/SiO2, Al2O3/SiO2, Journal of Mass Spectrometry, 45 (2010) 750-761.
[44] K. Kulyk, B. Palianytsia, J.D. Alexander, L. Azizova, M. Borysenko, M. Kartel, M. Larsson, T. Kulik, Kinetics of Valeric Acid Ketonization and Ketenization in Catalytic Pyrolysis on Nanosized $SiO_2$, $\gamma$-$Al_2O_3$, $CeO_2/SiO_2$, $Al_2O_3/SiO_2$ and $TiO_2/SiO_2$, ChemPhysChem, 18 (2017) 1943-1955.
[45] T.V. Kulik, N.O. Lipkovska, V.M. Barvinchenko, B.B. Palyanytsya, O.A. Kazakova, O.O. Dudik, A. Menyhárd, K. László, Thermal transformation of bioactive caffeic acid on fumed silica seen by UV–Vis spectroscopy, thermogravimetric analysis, temperature programmed desorption mass spectrometry and quantum chemical methods, Journal of Colloid and Interface Science, 470 (2016) 132-141.
[46] K. Kulyk, M. Borysenko, T.V. Kulik, L. Mikhalovska, J.D. Alexander, B. Palianytsia, Chemisorption and thermally induced transformations of polydimethylsiloxane on the surface of nanoscale silica and ceria/silica, Polymer Degradation and Stability, 120 (2015) 203-211.
[47] K. Kulyk, H. Zettergren, M. Gatchell, J.D. Alexander, M. Borysenko, B. Palianytsia, M. Larsson, T. Kulik, Dimethylsilanone Generation from Pyrolysis of Polysiloxanes Filled with Nanosized Silica and Ceria/Silica, ChemPlusChem, 81 (2016) 1003-1013.
[48] N.A. Nevskaya, Y.N. Chirgadze, Infrared spectra and resonance interactions of amide-I and II vibrations of α-helix, Biopolymers, 15 (1976) 637-648.
[49] S. Krimm, J. Bandekar, Vibrational Spectroscopy and Conformation of Peptides, Polypeptides, and Proteins, in: J.T.E. C.B. Anfinsen, M.R. Frederic (Eds.) Advances in Protein Chemistry, Academic Press1986, pp. 181-364.
[50] E. Vass, M. Hollósi, F. Besson, R. Buchet, Vibrational Spectroscopic Detection of Beta- and Gamma-Turns in Synthetic and Natural Peptides and Proteins, Chem Rev, 103 (2003) 1917-1954.
[51] P.I. Haris, D. Chapman, Does Fourier-transform infrared spectroscopy provide useful information on protein structures?, Trends Biochem Sci, 17 (1992) 328-333.
[52] J. Bandekar, Amide modes and protein conformation, BBA-Protein Struct M 1120 (1992) 123-143.
[53] L.J. Bellamy, The infrared spectra of complex molecules: advances in infrared group frequencies, Chapman and Hall 1980.
[54] D. Herbert, P.J. Phipps, R.E. Strange, Chapter III Chemical Analysis of Microbial Cells, in: J.R. Norris, D.W. Ribbons (Eds.) Methods in Microbiology, Academic Press1971, pp. 209-344.
[55] R.A. Nyquist, Interpreting Infrared, Raman and Nuclear Magnetic Resonance Spectra: Variables in data interpretation of infrared and Raman spectra, Academic Press2001.
[56] V. Wittmann, Glycopeptides and Glycoproteins: Synthesis, Structure, and Application, Springer 2007.